IMPROVED FORMULAE FOR LOW-FREQUENCY ULTRASONIC ATTENUATION IN METALS

ANUBHAV ROY* AND CHRISTOPHER M. KUBE†

ABSTRACT

A range of ultrasonic techniques associated with the nondestructive evaluation of metals involves the propagation of low-frequency elastic waves. Metals that are isotropic and homogeneous in the macroscopic length scale contain elastic heterogeneities, such as grain boundaries within the microstructures. Ultrasonic waves propagating through such microstructures get scattered from the grain boundaries. As a result, the propagating ultrasound attenuates. The mass density and the elastic anisotropy in each constituent grain govern the degree of heterogeneity in the polycrystalline aggregates. Existing elastodynamic models consider first-order scattering effects from grain boundaries. This paper presents the improved attenuation formulae, for the first time, by including the next order of grain scattering effects. Results from investigating 759 polycrystals reveal a positive correlation between the effects of higher-order scattering from grain boundaries and the degree of heterogeneity. Thus, higher-order grain scattering effects are now known. These results motivate further investigation into higher frequencies and strongly scattering alloys in the future.

KEYWORDS: ultrasound, microstructures, grain boundaries, scattering, attenuation

* Graduate Student, Department of Engineering Science and Mechanics, The Pennsylvania State University, University Park, PA 16802, USA; anubhav199421@gmail.com
† Assistant Professor, Department of Engineering Science and Mechanics, The Pennsylvania State University, University Park, PA 16802, USA

Materials Evaluation 82 (6): 34–40
https://doi.org/10.32548/2024.me-04422

Introduction

Metals are aggregates of crystalline grains that appear in different shapes, sizes, and orientations. The contrasts in grain orientations result in a variation in the elastic stiffness across the boundaries that separate any neighboring grains. Spatial variation in the elastic stiffness causes the propagating ultrasonic waves to scatter due to reflections and refractions at those grain boundaries. Cumulative events of scattering associated with the evolution of secondary waves from the grain boundaries cause the ultrasonic waves to attenuate. Moreover, the ultrasonic waves propagating in polycrystalline metals can get mode converted while scattering from the grain boundaries depending on the respective speed and angle of incidence. Thus, it is essential to distinctly determine the attenuation for the propagation of longitudinal and transverse waves within the heterogeneous microstructures. The scattering of an incident longitudinal wave from a typical grain boundary and its subsequent mode conversion is presented using a schematic diagram in Figure 1. The left-hand side of Figure 1 shows a synthetic polycrystalline microstructure generated by Dream3D [1]. The contrasts in color represent different orientations of the grain. The grain orientation distribution is Gaussian random, corresponding to the statistical isotropy in the medium. The right-hand side of Figure 1 shows the scattering due to refraction at a typical grain boundary in a magnified scale. The vertical solid arrow shown on the right-hand side of Figure 1 represents the longitudinal waves incident on the

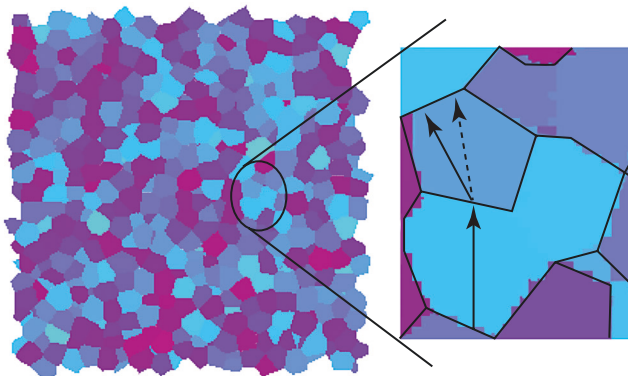

Figure 1. The vertical black arrow in the right image shows an incident longitudinal wave upon a grain boundary. The wave refracts into a longitudinal wave and a mode-converted transverse wave.

grain boundary. Part of those incident waves get mode converted into transverse waves, as shown by the dashed arrow. In contrast, the rest gets transmitted as a longitudinal wave, denoted by the oblique solid arrow, into the neighboring grain.

Rayleigh [2] was one of the first to address the propagation of elastic waves in solids that possess a spatial variation in mechanical properties. Earlier, Rayleigh [3] introduced an approximation to consider only the fundamental frequency corresponding to the first mode of free vibration in systems with n degrees of freedom. This low-frequency Rayleigh approximation [3] was inherent in modeling the inhomogeneous media [2] since the latter assumed the heterogeneities to be small and spherical compared to the wavelength of the propagating elastic waves. Moreover, the elastic medium was assumed to be isotropic for mathematical simplicity. Rayleigh's model [2] shows the intensity of the secondary fields, evolving due to scattering from the "small obstacles" to possess a fourth-power relationship with the frequency of propagating elastic waves. The nonzero intensity of these secondary fields can be manifested as attenuation of the propagating primary waves. One of the earliest attenuation measurements was provided by Mason and McSkimin [4] for the propagation of low-frequency ultrasound in aluminum and glass rods. The frequencies of propagation in Mason and McSkimin's experiments [4] were maintained in the range of 2–15 MHz. The attenuation measurements by Mason and McSkimin [4] echo Rayleigh's estimates regarding the fourth-power relationship with the propagation frequency. The experimental observations by Mason and McSkimin [4] further set an upper limit on the obstacle size to be a third of the wavelength for the validity of this fourth-power law. Following the experimental measurements, Mason and McSkimin [5] provided theoretical estimates of attenuation for single scattering from an obstacle that is too small and too large in size relative to the wavelength corresponding to propagation in the so-called Rayleigh and the geometric regimes, respectively. The theoretical estimates reveal the attainment of respective asymptotes for elastic wave dispersion in both these regimes. Huntington [6] observed a transitional behavior between these two asymptotes in the so-called stochastic scattering regime. However, the dispersion behavior for frequencies beyond the Rayleigh limit is beyond the scope of this paper.

The seminal work by Weaver [7] models the wave displacement at a point as a Green's function dyadic in response to a 3D impulse created at another point in the polycrystalline microstructure. This model [7] is more general than the one by Mason and McSkimin [5] for including multiple scattering effects. Weaver's model [7] solves for the mean wave propagation across polycrystalline microstructures analogous to the Unified Theory by Stanke and Kino [8]. However, the Unified Theory [8] assumes the propagation of a 3D plane wave. In contrast, Weaver's model [7] is free from any such assumption. Weaver's model [7] truncates the elastodynamic Dyson series constituted by the so-called mass operators, which capture the scattering within bulk polycrystals. This directly allows Weaver's model [7] to provide estimates of important parameters like scattered intensity, diffusivity, and so forth, for ultrasonic propagation through different polycrystals. Nevertheless, equivalent to the Keller approximation–based homogenization considered in the Unified Theory [8], Weaver's model [7] considers a first-order smoothing approximation (FOSA)–based truncation of the mass operator series to the leading term. Moreover, Weaver [7] considers the Born approximation associated with substituting the real part of the heterogeneous wavenumber by the wavenumber in the corresponding homogeneous medium. However, this restricts the applicability of the Born-FOSA model [7] to the geometric scattering regime. Nevertheless, for frequencies in the Rayleigh and the majority of the stochastic regime, the attenuation estimates from the Born-FOSA model [7] agree well with the Unified Theory [8], which is free from the Born approximation. Thus, it is reasonable to adopt Weaver's model [7] for applications that include the propagation of low-frequency ultrasound. Over the years, the FOSA model [7] has been applied to estimate scattering within different heterogeneous microstructures. Turner [9] used the FOSA model [7] for polycrystals possessing texture or a bias in grain orientation distribution. The estimates from Turner's model [9] agree well with the ones from Ahmed and Thompson [10], which, on the other hand, apply the Unified Theory [8] for the textured aggregates. Yang and Turner [11, 12] used the FOSA model [7] to provide estimates of attenuation due to the presence of damage and periodic cracks within the microstructures. Kube and Turner [13] investigated the effects of initial/residual stresses on the attenuation estimates in polycrystals by using the FOSA model [7]. However, equivalent to the Unified Theory [8], the FOSA model [7] considers first-order correlations between the grain boundaries to estimate attenuation in statistically isotropic and homogeneous metals composed of randomly distributed cubic grains. The anisotropy within each constituent grain is considered the sole source of heterogeneity in these models. The crystallite anisotropy in metals like iron or lithium is considerably higher than in aluminum. Significant discrepancies are observed by Sha et al. [14] and Huang et al. [15] while comparing the existing FOSA-based estimates [7, 8] against more computationally expensive finite element (FE) simulations of low-frequency longitudinal wave propagation in metals with high crystallite anisotropy. Since the FE models inherently include multiple orders of scattering, Sha et al. [14] and Huang et al. [15] attribute the observed discrepancies to the homogenization associated with the FOSA-based truncation [7, 8]. Moreover, the recent observations by Cook et al. [16] on porous additively manufactured metals motivate the investigation of correlations between crystallite anisotropy and accuracy in the existing attenuation estimates.

Thus, for the first time, this paper includes a third-order smoothing approximation (TOSA)–based truncation of the elastodynamic Dyson series to quantify the effects of higher-order multiple scattering from the grain boundaries during ultrasonic propagation in metals. This paper investigates the accuracy of the existing FOSA-based estimates [7] by

adding two terms corresponding to TOSA for low-frequency (Rayleigh) propagation in cubic polycrystals. The Rayleigh scattering regime is associated with elastic wave propagation of low normalized frequency or wavenumber. Within the Rayleigh limit, it is reasonable to assume the two-point correlation function to be independent of the magnitude of the scattered wave vector [7, 8], which leads to closed-form attenuation expressions. Considering the so-called Born approximation [7], this paper includes closed-form attenuation formulae for low-frequency propagation of longitudinal and transverse waves corresponding to the FOSA- and TOSA-based truncation of the governing Dyson series. Finally, this paper highlights the effects of including the TOSA-based multiple scattering terms into the current model as a comparison against the existing FOSA model in terms of the attenuation estimates in 759 different cubic polycrystals, including common metals like aluminum, iron, and lithium.

Theory

Statistical homogeneity describes the heterogeneous elastic stiffness by an effective stiffness of a corresponding homogeneous medium. The ensemble average of the heterogeneous stiffness is manifested as this effective homogeneous stiffness under the assumptions of statistical homogeneity. Thus, the heterogeneous elastic stiffness tensor $\mathbf{C}(\mathbf{x})$ can be defined as:

$$\mathbf{C}(\mathbf{x}) = \mathbf{C}_0 + \boldsymbol{\gamma}(\mathbf{x}) \quad (1)$$

where

$\mathbf{C}_0$ represents the elastic stiffness tensor of the statistically homogeneous medium, and

$\boldsymbol{\gamma}(\mathbf{x})$ denotes the spatial variation in the elastic stiffness.

Moreover, the Ergodic hypothesis allows the representation of the ensemble average of a quantity by its volumetric average. Thus, $\mathbf{C}_0$ represents the spatially averaged elastic stiffness in the polycrystalline medium. Wave displacement at a point, $\mathbf{x}$, along the i^{th} direction at time $t > 0$ can be modeled as a spatio-temporal Green's function dyadic, $G_{ij}(\mathbf{x}, \mathbf{x}', t)$, for producing a 3D impulse, $\delta^3(\mathbf{x} - \mathbf{x}')$, at a source $\mathbf{x}'$ along the j^{th} direction at time $t = 0$. Neglecting the temporal absorption, conservation of linear momentum leads to the governing equation as:

$$\left[\frac{\partial}{\partial \mathbf{x}}\left(\mathbf{C}(\mathbf{x})\frac{\partial}{\partial \mathbf{x}}\right) - \rho\omega^2\right]\mathbf{G}(\mathbf{x}, \mathbf{x}') = \mathbf{I}\,\delta^3(\mathbf{x} - \mathbf{x}') \quad (2)$$

where

$\mathbf{I}$ represents an identity matrix,

ρ denotes the uniform mass density, and

ω is the angular frequency of the propagating wave in the corresponding homogeneous medium.

However, the solution of wave displacement between any two specific points in the microstructure is intractable using Equation 2. Nevertheless, the governing equation is solvable in a statistical sense. Thus, the ensemble average of Equation 2 leads to the elastodynamic Dyson equation:

$$\langle \mathbf{G}(\mathbf{x}, \mathbf{x}') \rangle = \mathbf{G}^0(\mathbf{x}, \mathbf{x}') + \iint \mathbf{G}^0(\mathbf{x}, \mathbf{x}_1)\mathbf{m}(\mathbf{x}_1, \mathbf{x}_r)\langle \mathbf{G}(\mathbf{x}_r, \mathbf{x}') \rangle\, d^3\mathbf{x}_1\, d^3\mathbf{x}_r \quad (3)$$

which decomposes the mean wave propagation, $\langle \mathbf{G} \rangle$ into a homogeneous part, $\mathbf{G}^0$, and a scattered part. The scattered part contains the mass operator, $\mathbf{m}$, responsible for capturing all information about heterogeneity in the medium. Equation 3 can be iterated by substitution of the mean displacement, $\langle \mathbf{G} \rangle$, term on the right-hand side. Subsequent iterations produce the mass operator series that can be shown using the Feynman diagrams as:

(4)

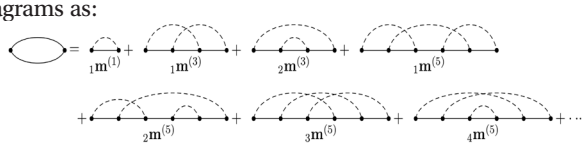

It is common in the existing homogenization literature [17, 18] to assume the spatial distribution of the fluctuation, $\boldsymbol{\gamma}$, as Gaussian, which eliminates all mass operator diagrams corresponding to the odd-moment correlations shown by Frisch [19] and retains only the even-point mass operator diagrams as shown in Equation 4. The leading term, $_1\mathbf{m}^{(1)}$, of the series shown in Equation 4 contributes the most converged by diminishing contributions from the following terms. Thus, truncating this mass operator series shown in Equation 4 to a certain term corresponds to homogenizing the heterogeneous medium to a certain extent. Existing elastodynamic models truncate the series to the first term, $_1\mathbf{m}^{(1)}$, corresponding to the FOSA. For the first time, the current analytical model includes the two TOSA-based terms, $_1\mathbf{m}^{(3)}$ and $_2\mathbf{m}^{(3)}$, to investigate the necessity of considering higher-order correlations between the grain boundaries. Any two points (or grain boundaries) connected by the dashed loops in the mass operator diagrams shown in Equation 4 are considered to possess a statistical correlation since they belong to the same grain. This correlation depends on different physical parameters, including the grain orientation distribution, elastic properties, grain size distribution, and so forth. Expressions for attenuation (α) are normalized with respect to twice the correlation length (2ℓ), related to the average grain diameter of the polycrystal. The normalized attenuation in equiaxed polycrystals composed of cubic crystallites depends on three parameters: (a) the degree of heterogeneity, ϵ, (b) the wavespeed ratio, K, and (c) the normalized wavenumber, x_0. The degree of heterogeneity in polycrystalline microstructure depends on the bulk wavespeed in the homogeneous medium (c_0), density (ρ), and the three independent stiffness components (c_{11}, c_{12}, c_{44}) of the constituent cubic crystallites. The longitudinal and transverse degrees of heterogeneities can be defined [8] as:

$$\epsilon_L = \frac{1}{\langle c_{11} \rangle}\sqrt{\frac{4}{525}\left(c_{11} - c_{12} - 2c_{44}\right)^2} = \frac{1}{\rho c_{0L}^2}\sqrt{\frac{4}{525}\left(c_{11} - c_{12} - 2c_{44}\right)^2} \quad (5)$$

$$\epsilon_T = \frac{1}{\langle c_{44} \rangle}\sqrt{\frac{3}{700}\left(c_{11} - c_{12} - 2c_{44}\right)^2} = \frac{1}{\rho c_{0T}^2}\sqrt{\frac{3}{700}\left(c_{11} - c_{12} - 2c_{44}\right)^2} \quad (6)$$

where

the angle brackets $\langle\cdot\rangle$ represent Voigt-averaged quantities.

The ratio (K) between the longitudinal and transverse wavespeeds, c_{0L} and c_{0T}, respectively, in the homogeneous medium is defined [7] as:

$$(7)\quad K = \frac{c_{0L}}{c_{0T}}$$

The correlation length (ℓ) normalized wavenumber x_0 can be expressed as:

$$(8)\quad x_0 = \ell\, p_0 = \frac{2\pi\ell f}{c_0}$$

where

p_0 is the wavenumber, and

f is the frequency of the propagating wave in the corresponding homogeneous medium.

It is to be noted that Equation 8 applies to either a longitudinal or transverse wave mode, which will be denoted with an L or T subscript, respectively. The Rayleigh scattering regime corresponds to frequencies such that the square of the normalized wavenumber is much less than 1, that is, $x_0^2 << 1$. The wavenumber in a homogeneous medium (p_0) is real, while that in a heterogeneous medium (p) is complex. The real part of this complex wavenumber p is related to wavespeed, while the imaginary counterpart is related to attenuation (α) in the heterogeneous medium. For frequencies within the Rayleigh limit, the real part of the wavenumber can be assumed to be dominated by the homogeneous wavenumber p_0. This assumption corresponds to the so-called Born approximation that replaces the real part of the heterogeneous wavenumber, $\Re(p)$, by p_0 to simplify the wavenumber solutions. From the wavenumber solution, attenuation can be calculated using $\alpha = \Im(p)$. Finally, under the assumptions of long wavelength (Rayleigh limit) [7], the closed-form expression for the FOSA-based normalized longitudinal attenuation $\left(2\ell\,\alpha^L_{FOSA}\right)$ can be shown [7] in terms of ϵ_L, x_{0L}, and K as:

$$(9)\quad 2\ell\,\alpha^L_{FOSA} = \frac{14}{5}\epsilon_L^2 x_{0L}^4\left(3K^5+2\right)$$

For a detailed derivation of the TOSA-based mass operators, readers are encouraged to refer to the dissertation by Roy [20]. Including TOSA in our current model, the improved formula for the normalized attenuation ($2\ell\,\alpha^L$) of the longitudinal waves can be written as:

$$(10)\quad 2\ell\,\alpha^L = 2\ell\,\alpha^L_{FOSA}\left[1+\frac{17\,\epsilon_L^2}{3600}\left(3K^2+2\right)^2\right]$$

where

$$\alpha^L = \alpha^L_{FOSA} + 2\alpha^L_{TOSA}.$$

The correction is easily observed in Equation 10 as the second term in the square brackets. Thus, the effect of improvement on longitudinal attenuation estimates for including TOSA in the current model can be expressed as a ratio:

$$(11)\quad \frac{\alpha^L}{\alpha^L_{FOSA}} = 1+\frac{17\,\epsilon_L^2}{3600}\left(3K^2+2\right)^2$$

Similarly, for transverse wave propagation, the expression for normalized attenuation ($2\ell\,\alpha^T_{FOSA}$) based on FOSA can be shown [7] in terms of ϵ_T, x_{0T}, and K as:

$$(12)\quad 2\ell\,\alpha^T_{FOSA} = \frac{56}{15}K^{-5}\epsilon_T^2 x_{0T}^4\left(3K^5+2\right)$$

and the current estimates of the normalized transverse attenuation $\left(2\ell\,\alpha^T\right)$ for including TOSA can be shown as:

$$(13)\quad 2\ell\,\alpha^T = 2\ell\,\alpha^T_{FOSA}\left[1+\frac{17\,\epsilon_T^2}{2025}\left(3+2K^{-2}\right)^2\right]$$

where

$$\alpha^T = \alpha^T_{FOSA} + 2\alpha^T_{TOSA}.$$

It is to be noted that Equation 13 includes a correction to the typographically erroneous expression reported as Equations 3.106 and 3.110 in the dissertation by Roy [20]. Nevertheless, following Equation 13, the factor representing the corresponding improvement for including TOSA on the transverse attenuation estimates can be shown by a ratio as:

$$(14)\quad \frac{\alpha^T}{\alpha^T_{FOSA}} = 1+\frac{17\,\epsilon_T^2}{2025}\left(3+2K^{-2}\right)^2$$

Comparison between Equations 11 and 14 by substituting the expressions for the degrees of heterogeneities shown in Equations 5 and 6 results in an identical contribution from the TOSA terms for longitudinal and transverse propagation as:

$$(15)\quad \frac{\alpha^L}{\alpha^L_{FOSA}} = \frac{\alpha^T}{\alpha^T_{FOSA}}$$

Results and Discussions

The utility of including the TOSA-based terms in the current model is studied on a range of untextured polycrystals composed of randomly distributed cubic grains possessing a wide spectrum of crystallite anisotropy for frequencies within the Rayleigh limit. From the available resources on density functional theory (DFT)-based calculations [21], 759 different materials have been considered with distinct crystallite stiffness components, c_{11}, c_{12}, c_{44}, and mass density ρ. The magnitude of the mass density relative to the crystallite anisotropy determines the degree of heterogeneity, as shown in Equations 5 and 6. Thus, each quartet, including the three stiffness and density constants, associates a unique degree of heterogeneity to each polycrystalline aggregate. The normalized wavenumber for this study is considered to be $x_0 = 0.01$, corresponding to the Rayleigh scattering regime. Results for some commonly used metals like aluminum, iron, and lithium for $x_0 = 0.01$ are

TABLE 1
Effect of including TOSA for estimating attenuation in common metals for $x_0 = 0.01$

Materials	K	ϵ_L	$2\ell\alpha^L \times 10^{-10}$	α^L/α^L_{FOSA}	ϵ_T	$2\ell\alpha^T \times 10^{-10}$	α^T/α^T_{FOSA}
Aluminum	2.02	0.0088	2.24	1.0000	0.0270	0.83	1.0000
Iron	1.83	0.0434	33.25	1.0013	0.1086	13.65	1.0013
Lithium	1.81	0.0737	92.05	1.0036	0.1811	38.15	1.0036

highlighted in Table 1 to demonstrate how these estimates are calculated for the propagation of both longitudinal and transverse waves.

Figure 2 reveals the effects of including TOSA terms on the attenuation estimates for the propagation of low-frequency (a) longitudinal ($x_{oL} = 0.01$) and (b) transverse ($x_{oT} = 0.01$) waves, respectively, in all the 759 aggregates. The longitudinal and transverse degrees of heterogeneity constitute the respective X axes of the plots shown in Figure 2. The effects of including the TOSA-based terms shown in Equations 11 and 14 are plotted along the respective Y axes in Figure 2. Both plots show a positive correlation between the higher-order

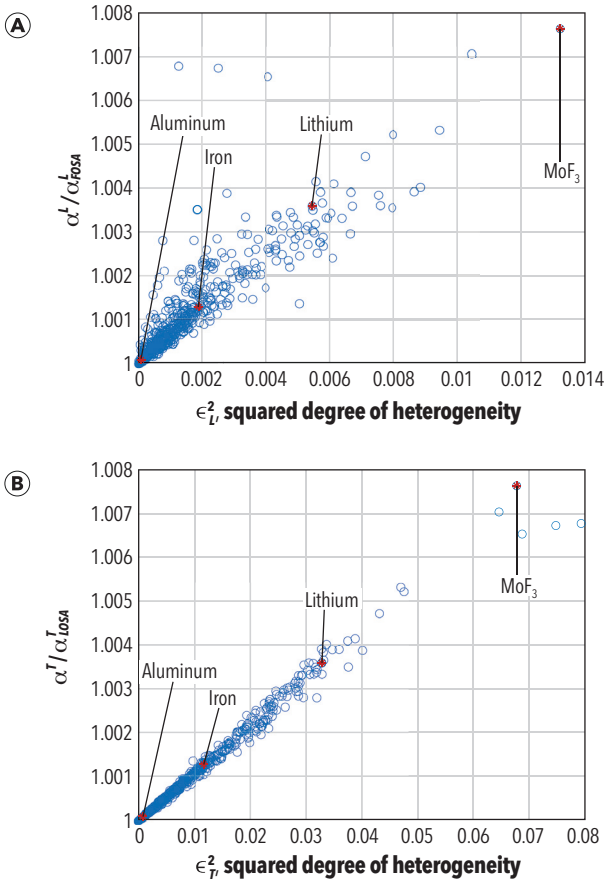

Figure 2. Effects of including TOSA in the formulation for attenuation of (a) longitudinal and (b) transverse waves through 759 different polycrystalline aggregates.

scattering effects on attenuation estimates and the degree of heterogeneity. The correlation is found to be sharper for the transverse wave propagation as compared to the longitudinal. The higher standard deviation in the results for longitudinal attenuation can be attributed to the dependence of longitudinal wavespeed, c_{oL}, in the homogeneous medium on both bulk and the transverse (shear) modulus, as opposed to the transverse wavespeed, c_{oT}, which depends solely on the transverse (shear) modulus. Some aggregates with characteristic degrees of heterogeneity are highlighted in the plots. The degrees of heterogeneity in aluminum and lithium can be considered to be two extremums among the metals: approximately 0.0088 and 0.0737, respectively, with iron falling in between having the same as 0.0434 for longitudinal propagation. In addition to these common metals tabulated in Table 1, molybdenum trifluoride (MoF_3) is highlighted due to the high anisotropy in the constituent crystallites associated with a longitudinal degree of heterogeneity of magnitude 0.115.

For aluminum, the ratio between current and existing FOSA-based estimates is almost equal to 1 for the propagation of both the longitudinal and transverse waves. This confirms that the FOSA model is sufficient to model elastic wave scattering in microstructures with low degrees of heterogeneity. However, with the increase in the degree of heterogeneity, the necessity for including higher-order scattering into the model is found to be increasing. For MoF_3, the effect on longitudinal and transverse attenuation estimates is found to be about 0.76%. Similarly, the effects of including the TOSA-based terms on longitudinal and transverse attenuation in common metals like iron and lithium are found to be about 0.13% and 0.36%, respectively. For using Born approximation, the effects of including higher-order scattering are identical for the propagation of the longitudinal and transverse waves. This does not hold true for solutions beyond the Born approximation, which is beyond the scope of the current communication. However, in Figure 2, the effect of including TOSA-based terms is observed to be anomalously high on the longitudinal attenuation estimates in the three metallic alloys that possess relatively low degrees of heterogeneity, namely, aluminum-vanadium (AlV_3), niobium-indium (Nb_3In), and hafnium-tin (HfSn). This dominant effect of higher-order scattering on specifically the longitudinal estimates in these materials can be attributed to their common trend of possessing high values of K beside the general issue regarding the high standard deviation.

Conclusions and Future Work

The effects of including higher-order statistical correlations between the grain boundaries are examined for the low-frequency attenuation estimates in cubic polycrystals. For the first time, the governing Dyson equation includes a TOSA-based homogenization of the mass operator series. The long wavelength (Rayleigh-limit) assumptions and the Born approximation are incorporated in the current model analogous to the existing FOSA model [7]. The closed-form expressions of attenuation corresponding to the FOSA- and TOSA-based truncations are presented for the propagation of low-frequency longitudinal and transverse waves. The current attenuation estimates from the TOSA model retain the fourth power relationship with the normalized frequency or wavenumber in the reference homogeneous medium. The effects of including the higher-order scattering terms in the Dyson series are presented as a ratio between the estimates from the current TOSA model and the existing FOSA model. These effects are studied for the longitudinal and transverse wave propagation in 759 equiaxed polycrystals corresponding to varying degrees of heterogeneity. The current model considers crystallite anisotropy as the sole source of heterogeneity. Almost no effect is observed for including the TOSA-based terms on the attenuation estimates in aluminum due to the low degree of heterogeneity. However, for polycrystals composed of increasingly anisotropic grains, this effect increases for longitudinal and transverse wave propagation within the bulk polycrystal. The effects are found to be 0.13%, 0.36%, and 0.76% for the propagation of longitudinal and transverse waves in iron, lithium, and molybdenum trifluoride, respectively, with normalized wavenumber, $x_0 = 0.01$. Thus, considering a Gaussian fluctuation distribution in elastic stiffness, the current results, for the first time, confirm that even for lithium, the order of homogenization involved in the FOSA-based estimates is insufficient to explain the extent of overestimation observed in the FE and semi-analytical results by Sha et al. [14] and Huang et al. [15]. However, investigation of the higher-order scattering effects for non-Gaussian fluctuation distributions, including the mass operator terms corresponding to the odd-moment correlations shown by Frisch [19], remains a future work. Moreover, due to consideration of the Born approximation, the effects for longitudinal propagation are indistinguishable from that for transverse propagation in these polycrystals. However, the correlation between the higher-order scattering effects and the degree of heterogeneity is sharper for transverse propagation than for longitudinal. This difference in standard deviation between the plots is attributed to the dependence of the longitudinal wavespeed on both bulk and transverse (shear) modulus as opposed to the transverse counterpart that solely depends on the transverse (shear) modulus.

Besides scattering from the grain boundaries, potential future work includes applying this TOSA model to investigate the higher-order scattering effects in microstructures possessing generally anisotropic grains, texture, periodic cracks, deformed grains, residual stresses, and multiple phases. Moreover, the higher-order scattering effects on the attenuation estimates are found insensitive to the mode of propagation due to consideration of the Born approximation, which can be relaxed in the future to obtain more realistic results. The effects of including TOSA on the attenuation estimates may increase with frequency. Thus, extending this model beyond the Rayleigh limit is necessary to explore the higher-order scattering effects for all three regimes until the geometric asymptote. Finally, the current model may generate opportunities to conduct more accurate nondestructive evaluation in metals, including propagation of low-frequency longitudinal and transverse waves.

ACKNOWLEDGMENTS

This work is supported by the National Science Foundation program NSF/ENG-UKRI EPSRC Opportunity under award 2225215. The authors acknowledge the American Society for Nondestructive Testing for the 2022 ASNT Fellowship Award.

REFERENCES

1. Groeber, M. A., and M. A. Jackson. 2014. "Dream. 3D: A digital representation environment for the analysis of microstructure in 3D." *Integrating Materials and Manufacturing Innovation* 3 (1): 56–72. https://doi.org/10.1186/2193-9772-3-5.

2. Rayleigh, J. W. S. B. 1896. *The theory of sound*. Vol. 2. Macmillan.

3. Rayleigh, J. W. S. B. 1873. *Some general theorems relating to vibrations*. London Mathematical Society.

4. Mason, W. P., and H. J. McSkimin. 1947. "Attenuation and scattering of high frequency sound waves in metals and glasses." *Journal of the Acoustical Society of America* 19 (3): 464–73. https://doi.org/10.1121/1.1916504.

5. Mason, W. P., and H. J. McSkimin. 1948. "Energy losses of sound waves in metals due to scattering and diffusion." *Journal of Applied Physics* 19 (10): 940–46. https://doi.org/10.1063/1.1697900.

6. Huntington, H. B. 1950. "On ultrasonic scattering by polycrystals." *Journal of the Acoustical Society of America* 22 (3): 362–64. https://doi.org/10.1121/1.1906613.

7. Weaver, R. L. 1990. "Diffusivity of ultrasound in polycrystals." *Journal of the Mechanics and Physics of Solids* 38 (1): 55–86. https://doi.org/10.1016/0022-5096(90)90021-U.

8. Stanke, F. E., and G. S. Kino. 1984. "A unified theory for elastic wave propagation in polycrystalline materials." *Journal of the Acoustical Society of America* 75 (3): 665–81. https://doi.org/10.1121/1.390577.

9. Turner, J. A. 1999. "Elastic wave propagation and scattering in heterogeneous, anisotropic media: Textured polycrystalline materials." *Journal of the Acoustical Society of America* 106 (2): 541–52. https://doi.org/10.1121/1.427024.

10. Ahmed, S., and R. B. Thompson. 1996. "Propagation of elastic waves in equiaxed stainless-steel polycrystals with aligned [001] axes." *Journal of the Acoustical Society of America* 99 (4): 2086–96. https://doi.org/10.1121/1.415395.

11. Yang, L., and J. A. Turner. 2003. "Elastic wave propagation and scattering in solids with uniaxially aligned cracks." *Journal of the Acoustical Society of America* 114 (2): 591–600. https://doi.org/10.1121/1.1592158.

12. Yang, L., and J. A. Turner. 2003. "Scattering of elastic waves in damaged media." *Journal of the Acoustical Society of America* 113 (6): 2992–3000. https://doi.org/10.1121/1.1570444.

13. Kube, C. M., and J. A. Turner. 2015. "Stress-dependent second-order grain statistics of polycrystals." *Journal of the Acoustical Society of America* 138 (4): 2613–25. https://doi.org/10.1121/1.4932026.

14. Sha, G., M. Huang, M. J. S. Lowe, and S. I. Rokhlin. 2020. "Attenuation and velocity of elastic waves in polycrystals with generally anisotropic grains: Analytic and numerical modeling." *Journal of the Acoustical Society of America* 147 (4): 2442–65. https://doi.org/10.1121/10.0001087.

15. Huang, M., P. Huthwaite, S. I. Rokhlin, and M. J. S. Lowe. 2022. "Finite-element and semi-analytical study of elastic wave propagation in strongly scattering polycrystals." *Proceedings - Royal Society. Mathematical, Physical and Engineering Sciences* 478 (2258): 20210850. https://doi.org/10.1098/rspa.2021.0850.

16. Cook, O., N. Huang, R. Smithson, C. Kube, A. Beese, and A. Argüelles. 2022. "Ultrasonic characterization of porosity in components made by binder jet additive manufacturing." *Materials Evaluation* 80 (4): 37–44. https://doi.org/10.32548/2022.me-04266.

17. Rytov, S. M., Y. A. Kravtsov, and V. I. Tatarskii. 1989. *Principles of Statistical Radiophysics: Wave Propagation Through Random Media*. Vol. 4. Springer.

18. Tsang, L., and J. A. Kong. 2004. *Scattering of electromagnetic waves: advanced topics*. John Wiley & Sons.

19. Frisch, U. 1968. *Wave propagation in random media, probabilistic methods in applied mathematics*. Vol. 1., 75–198. New York: Academic Press.

20. Roy, A. 2023. *Elastic Wave Propagation and Scattering in Polycrystals*. Doctoral Dissertation. The Pennsylvania State University. https://etda.libraries.psu.edu/catalog/23646axr1431.

21. de Jong, M., W. Chen, T. Angsten, A. Jain, R. Notestine, A. Gamst, M. Sluiter, et al. 2015. "Charting the complete elastic properties of inorganic crystalline compounds." *Scientific Data* 2(1): 1–13. https://doi.org/10.1038/sdata.2015.9.